Orthogonal fingerprinting for accurate and fast single-molecule mechanical profiling of proteins

Carolina Pimenta-Lopes[*,#], Carmen Suay-Corredera*, Diana Velázquez-Carreras, David Sánchez-Ortiz, Jorge Alegre-Cebollada*

Centro Nacional de Investigaciones Cardiovasculares Carlos III (CNIC), 28029 Madrid, Spain

*equal contribution
[#]current address: Department of Physiological Sciences, University of Barcelona, Spain
Correspondence to Jorge Alegre-Cebollada: jalegre@cnic.es

ABSTRACT

Force-spectroscopy by Atomic Force Microscopy (AFM) is the gold-standard method for nanomechanical characterization of proteins. However, AFM suffers from unavoidable interexperimental force calibration errors that make it challenging and time-consuming to study modulation of protein nanomechanics. Here, we develop orthogonal fingerprinting to track mechanical unfolding of two different proteins in the same AFM experiment, under the same calibration parameters. We show that the accuracy of orthogonal fingerprinting is independent of force calibration errors, reaching up to a 6-fold improvement with respect to traditional AFM. Importantly, this improvement in accuracy is preserved even when unfolding force data are obtained from multiple, independent orthogonal fingerprinting experiments. We also demonstrate that orthogonal fingerprinting can speed up data acquisition more than 30 times. Benefiting from the increased accuracy of orthogonal fingerprinting, we determine that the mechanical stability of a protein is independent of its neighboring domains.

INTRODUCTION

The response of proteins to pulling forces is a main determinant of the stiffness of tissues, and is at the basis of cellular mechanosensing and mechanotransduction [1-4]. Similarly, the mechanics of protein/ligand interactions is tailored to their specific biological requirements [5-7]. Inspired by these biological insights, novel protein hydrogels with customized mechanical properties have been designed based on the nanomechanics of the constituent proteins [8,9]. Both the understanding of mechanobiological phenomena and the design of protein biomaterials require accurate determination of nanomechanical properties of proteins.

Single-molecule force-spectroscopy by atomic force microscopy (AFM) is the technique of choice to characterize protein nanomechanics due to its high length and time resolutions, straightforward experimental configuration and user friendliness [10]. In addition, the possibility to do force-spectroscopy AFM under force-clamp conditions enables detailed characterization of the underlying energy landscapes that govern protein behavior under force [11].

In force-spectroscopy AFM, molecular tethers involving the protein of interest are established between a surface and a flexible cantilever (Figure 1A, Supplementary Figure 1). Using piezoelectric elements, the surface and the cantilever are pulled apart with sub-nanometer resolution, leading to application of mechanical force to the molecular tether [12]. The magnitude of the pulling force sensed by the tether is determined from the deflection of a laser beam focused on the cantilever, as detected by a split photodetector. Mechanical force is calculated from the laser deflection signal thanks to calibration routines that estimate the spring constant of the cantilever (k_{sc}) [13]. Different calibration methods to estimate spring constants of AFM cantilevers have been developed, which differ in their simplicity, associated uncertainty, experimental compatibility and damage to the cantilever tip. In single-molecule AFM, calibration based on the analysis of the cantilever's thermal fluctuations is the common choice due to its compatibility with experimental requirements and overall ease of use. However, this method entails a 15-20% uncertainty especially for recently developed high-speed cantilevers [11,13-15]. Such calibration uncertainty leads to inaccurate determination of nanomechanical parameters. Hence, comparative studies between two experimental conditions that require different calibrations (e.g. nanomechanical changes induced by mutations, posttranslational modifications, or the protein context [16-19]), become challenging. Taking into account that mutations associated with development of disease can induce changes in protein unfolding forces as small as 10% [20], there is a pressing need to develop methods that can overcome limitations associated with inaccurate force calibration in AFM. The traditional approach to increase statistical power is to repeat AFM experiments, since individual calibration errors are more probable to be averaged out as more experiments are analyzed [21]. The drawback is a considerable loss of throughput of the technique.

It has been proposed that if two proteins are measured in the same AFM experiment, under the same calibration parameters, the limitations coming from uncertain calibration could be avoided [15,22,23]. In addition, simultaneous measurement would increase the throughput of force-spectroscopy AFM. Here, we use protein engineering, single-molecule AFM mechanical measurements, error propagation analysis, and Monte Carlo simulations to understand how cantilever calibration errors impact determination of nanomechanical properties by AFM, and develop orthogonal fingerprinting as a simple and widely applicable strategy for simultaneous measurement of proteins under the same force calibration. Orthogonal fingerprinting leads to drastically improved accuracy and throughput of single-molecule force-spectroscopy AFM.

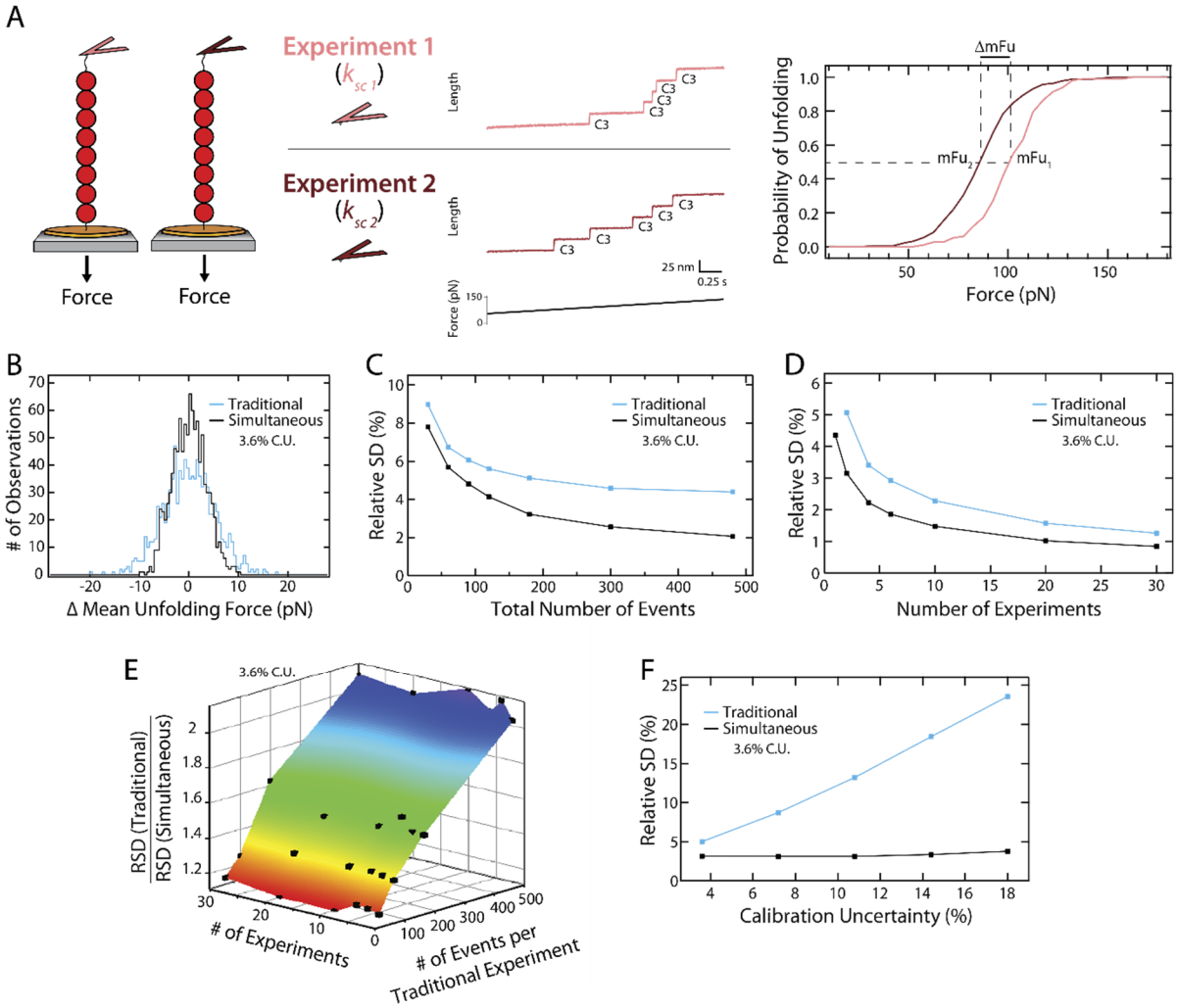

Figure 1. Simultaneous mechanical profiling of proteins by AFM circumvents inaccurate force calibration. (A) *Left:* Schematic representation of the traditional strategy to measure mechanical stability of proteins by AFM, in which data are obtained in multiple AFM experiments under different force calibration parameters (see also Supplementary Figure 1). *Middle*: Results from two independent AFM experiments in which a $(C3)_8$ polyprotein is pulled under a 40 pN/s linear increase in force. Due to uncertain calibration of the cantilever's spring constant k_{sc}, force values are affected by errors that differ between experiments. We show two individual unfolding traces of the $(C3)_8$ polyprotein, in which mechanical unfolding events of individual C3 domains are detected by increases of 24 nm in the length of the polyprotein. *Right*: Experimental cumulative unfolding probability distributions obtained from 117 (Experiment 1) and 191 (Experiment 2) C3 unfolding events. The corresponding mF_u values are 98.7 and 82.9 pN, respectively. **(B)** Distributions of ΔmF_u obtained by Monte Carlo simulations, considering the same total number of experiments and unfolding events for both traditional (blue) and simultaneous measurements (black). We considered 2 experiments, 200 unfolding events per protein, and a 3.6% calibration uncertainty (C.U.) **(C)** Keeping the number of experiments constant, the relative standard deviations (RSD) of the distribution of ΔmF_u decrease with the total number of unfolding events both in traditional (blue) and in simultaneous measurements (black). **(D)** Keeping the same number of events per experiment, the RSD of the distribution of ΔmF_u decreases with the number of experiments (blue: traditional strategy; black: simultaneous measurements). **(E)** The relative improvement in the RSD of ΔmF_u distributions obtained by the simultaneous strategy increases with the number of events per experiment, and remains fairly insensitive to the number of averaged experiments. **(F)** RSD of the distributions of ΔmF_u at increasing calibration uncertainties for the traditional (blue) and the simultaneous (black) strategies. The remaining simulation parameters are the same as in panel B. In panels B-F, the number of events per experiment and protein in the simultaneous approach was half of the number of events in the traditional strategy so that RSDs were compared between conditions with equal total number of events.

RESULTS

Interexperimental variation in unfolding forces in traditional AFM

To quantify variation in mechanical parameters obtained by AFM, we first examined the same protein in different, independently calibrated AFM experiments. We produced a polyprotein containing eight repetitions of the C3 domain of cardiac myosin-binding protein C (Supplementary Figure 2, Supplementary Text 1) and subjected individual $(C3)_8$ polyproteins to a linear increase in force of 40 pN/s using a force-clamp atomic force microscope. Results from two such independent experiments are shown in Figure 1A. Mechanical force triggers the unfolding of individual C3 domains. These unfolding events are detected as step increases in the length of the polyprotein of 24 nm (Figure 1A, middle; Supplementary Figure 3A). We determined the force at which the unfolding events occur and calculated distributions of unfolding forces. Despite the fact that both distributions are well defined (n > 115 events), the difference in their mean unfolding force (ΔmF_u) is 19% (Figure 1A, right). The magnitude of this interexperimental difference is in agreement with the spread of mF_u values reported in the literature for other proteins [21]. These differences can mask comparable changes in mechanical properties induced by biochemical cues, such as mutations or posttranslational modifications, which is an important limitation of traditional single-molecule AFM.

Interexperimental variations in mF_u are typically interpreted in terms of different errors in the calibration of AFM cantilevers, a procedure that can entail 20% uncertainty [11,13-15]. We used Monte Carlo simulations to examine how errors arising from uncertain cantilever calibration propagate to ΔmF_u. To this aim, in each simulated experiment we impose an error to the force that is randomly drawn from a normal distribution with a given Relative Standard Deviation (RSD) (See Methods). After definition of the error in force, a kinetic Monte Carlo algorithm is used to obtain a distribution of unfolding forces for a given number of protein domains subjected to a nominal 40 pN/s increase in force. For each one of the 1,000 cycles of the simulation, we calculate the corresponding ΔmF_u between two identical proteins considering a certain number of independent experiments, each one affected by a different error in force. Simulations return the distribution of ΔmF_u values obtained in the 1,000 cycles. The spread of the distribution is quantified by its RSD.

Using our Monte Carlo procedure, we have simulated mechanical protein unfolding under a 3.6% force calibration uncertainty, which is a reasonable estimate of the lowest uncertainty that the calibration by thermal fluctuations can achieve (Supplementary Text 2 and Supplementary Figure 4). Figure 1B shows the simulated distribution of ΔmF_u obtained from two traditional AFM experiments with different calibrations (200 unfolding events per experiment). We observe that the distribution of ΔmF_u is wider than expected just considering the imposed uncertainty in calibration (5.0% *vs.* 3.6%), as expected from the limited definition of the distribution of unfolding forces caused by the finite number of unfolding events. It is remarkable that two mean unfolding forces obtained in different cycles can differ by more than 25% (see also Supplementary Figure 5A). Hence, although conservative, a mere 3.6% inaccuracy in cantilever calibration can explain considerably higher differences in mF_u obtained in traditional AFM experiments.

Accuracy of multiple simultaneous AFM experiments is insensitive to calibration uncertainty

It has been argued that determination of ΔmF_u using a single cantilever, in the same experiment, could minimize the error associated with force calibration [15,22,23]. However, to the best of our knowledge, the resulting improvement in accuracy has not been quantified. We have used our

Monte Carlo simulations to estimate the accuracy achieved by simultaneous measurement of mechanical unfolding of two proteins. Considering equal total number of events and experiments, we find that determination of ΔmF_u in simultaneous experiments results in a decrease in RSD from 5.0% to 3.2% at a 3.6% calibration uncertainty (Figure 1B). The RSD of the ΔmF_u distribution obtained in simultaneous experiments is further reduced at higher number of unfolding events, as expected from better definition of the distribution of unfolding forces (Figure 1C, Supplementary Figure 5B). Unexpectedly, averaging multiple experiments in which both proteins are probed simultaneously leads to further reductions in RSD, despite the fact that each individual experiment is performed under different calibration parameters (Figure 1D). Increasing the number of events or experiments also results in better accuracy when proteins are probed in traditional, separate experiments (Figure 1 C,D). We find that the relative improvement in accuracy achieved by simultaneous measurement over traditional AFM increases with the number of events per experiment, and remains fairly constant with the number of experiments (Figure 1E). Hence, we conclude that averaging independent AFM experiments in which two proteins are probed simultaneously retains statistical power, even if those experiments are affected by different calibration errors.

All our simulations above consider a 3.6% uncertainty in force calibration, which is a much smaller value than usually reported [11,13-15]. Hence, we estimated the RSD of the distribution of ΔmF_u at increasing calibration uncertainties. As expected, higher calibration uncertainties lead to much increased RSD in traditional AFM, whereas the RSD of simultaneous measurements remains insensitive to the calibration uncertainty, even when data from several independent experiments are averaged (Figure 1F, Supplementary Figure 6A).

Orthogonal fingerprinting enables simultaneous characterization of proteins by AFM

Results in Figure 1D show that under a modest 3.6% uncertainty in force, simultaneous measurement can reach the same level of accuracy with 2-4 times less experiments than the traditional approach. Furthermore, at high values of calibration uncertainty, the accuracy by simultaneous measurements can be 6 times higher than in the traditional approach (Figure 1F). These remarkable improvements in throughput and accuracy prompted us to design a general strategy that enables simultaneous measurement of mechanical properties of proteins.

A fundamental requirement of force-spectroscopy AFM is to have reliable methods to identify single-molecule events. In the case of mechanical characterization of proteins, this requirement is fulfilled by the use of polyproteins, which provide molecular fingerprints that easily discriminate single-molecule events from spurious, non-specific interactions [24,25] (Supplementary Figure 3). As exemplified in Figure 1A, mechanical unfolding of polyproteins produce repetitive events whose length fingerprints the domain of interest. If two polyproteins are to be measured in the same experiment, it is imperative that they have different fingerprinting unfolding lengths. Here, we propose a widely applicable manner of achieving such orthogonal fingerprinting (OFP) through the use of heteropolyproteins, in which marker proteins are fused to the proteins of interest [26]. Since OFP identifies molecules through the unfolding length of the marker domains, proteins of interest to be compared in simultaneous AFM measurements can have the same unfolding length (e.g. mutant proteins).

To test whether heteropolyproteins can be employed to achieve OFP during simultaneous measurement of proteins by AFM, we first followed a single-marker strategy using the heteropolyprotein $(C3\text{-}L)_4$ (Figure 2, Supplementary Figure 2 and Supplementary Text 1). In

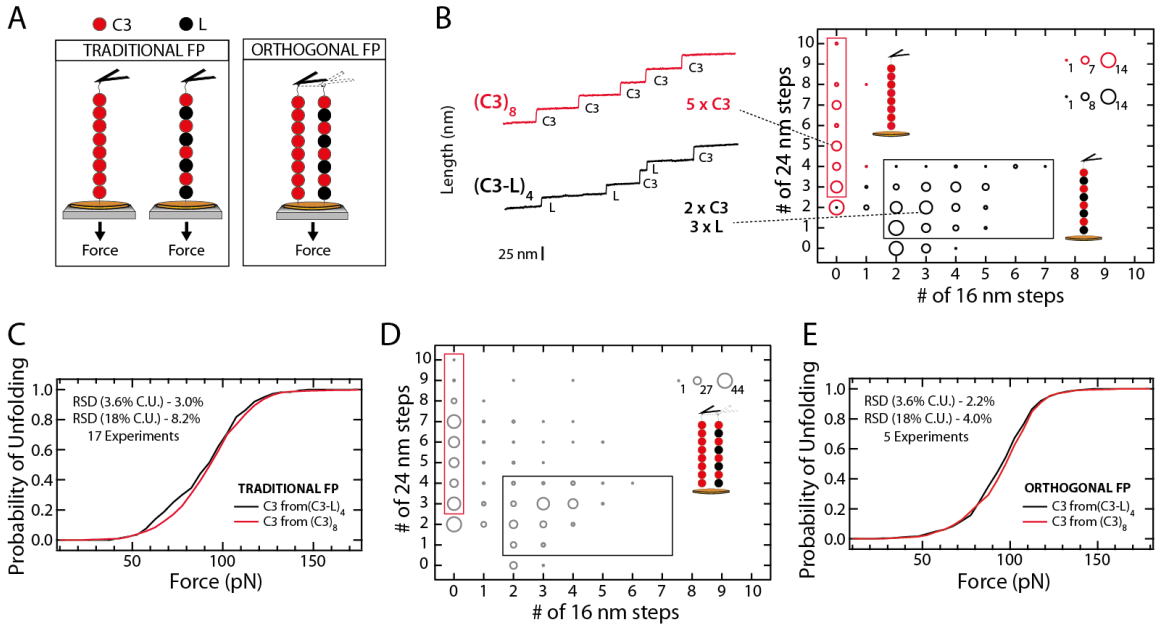

Figure 2. Single-marker orthogonal fingerprinting enables simultaneous measurement of proteins in AFM. (A) Schematic representation of the traditional and orthogonal fingerprinting (FP) strategies. *Left*: in traditional FP, $(C3)_8$ and $(C3\text{-}L)_4$ are measured in different AFM experiments. *Right*: In orthogonal FP both polyproteins are measured in the same experiment, under the same calibration parameters. **(B)** *Left*: representative unfolding traces of one $(C3)_8$ molecule (red) in which five 24 nm unfolding events are detected, and one $(C3\text{-}L)_4$ polyprotein (black) in which two 24 nm and three 16 nm unfolding events are observed. *Right*: Mechanical unfolding of $(C3)_8$ (red) and $(C3\text{-}L)_4$ (black) were measured in separate experiments. Individual traces were classified according to the number of 16 and 24 nm steps they contain. The plot shows the frequency of the traces that have different combinations of unfolding events, as indicated by the size of the dots. The rectangles represent gating strategies that unequivocally identify traces coming from $(C3)_8$ or $(C3\text{-}L)_4$. **(C)** Experimental cumulative unfolding probability distribution of the C3 domain in the context of $(C3)_8$ (11 experiments, 1334 events, red) and $(C3\text{-}L)_4$ (6 experiments, 177 events, black). The proteins were measured in different experiments following TFP. **(D)** $(C3)_8$ and $(C3\text{-}L)_4$ polyproteins were simultaneously measured in the AFM. Resulting traces were classified according to the number of 16 and 24 nm events they have. The gating criterion defined in panel B allows the classification of individual traces as resulting from $(C3)_8$ (red rectangle) or $(C3\text{-}L)_4$ (black rectangle). **(E)** Experimental cumulative unfolding probability distribution of the C3 domain in the context of $(C3)_8$ (625 events, red) and (C3-L)4 (311 events, black), calculated from unfolding data obtained in 5 independent OFP experiments. RSD values in panels C and E are estimated using Monte Carlo simulations that consider extreme values of calibration uncertainty (C.U.) (see also Supplementary Figure 7A). The pulling rate in all experiments was 40 pN/s.

$(C3\text{-}L)_4$, we used protein L as a marker since its unfolding length is different from the one of C3 [21]. Indeed, mechanical unfolding of $(C3\text{-}L)_4$ under a 40 pN/s ramp results in the appearance of 16 and 24 nm steps, which correspond, respectively, to the unfolding of L and C3 domains (Figure 2B, *left*, and Supplementary Figure 3B). We selected unfolding traces of $(C3)_8$ and $(C3\text{-}L)_4$, obtained in independent, traditional AFM experiments, and classified them according to the number of 16 and 24 nm events they contain. Our results show that a gating criterion of n(16nm) = 0 and n(24nm) > 2 unambiguously identifies unfolding events coming from $(C3)_8$, whereas events resulting from $(C3\text{-}L)_4$ can be safely assigned when n(16nm) > 1 and 0 < n(24nm) < 5 (Figure 2B, *right*). We analyzed 17 such traditional fingerprinting (TFP) experiments and obtained distributions of unfolding forces for C3 in the context of both polyproteins, which we found to be very similar (mF_u = 90. 7 and 88.4 pN for the homo and the heteropolyproteins, respectively, Figure 2C). We used our Monte Carlo simulations to estimate the RSD in ΔmF_u that is expected from the actual number of experiments and events obtained (RSD = 3.0% and 8.2% at 3.6% and 18% calibration uncertainties, respectively) (Supplementary Figure 7A, Supplementary Table 1).

Following validation of the polyprotein gating criterion (Figure 2B), we measured $(C3)_8$ and $(C3\text{-}L)_4$ simultaneously in OFP experiments. Single-molecule traces were classified according to the number of 16 and 24 nm steps they contain, and sorted as coming from the $(C3)_8$ or $(C3\text{-}L)_4$ before analysis of unfolding data (Figure 2D). Also in OFP, the distributions of unfolding probability of C3 in the context of $(C3)_8$ and $(C3\text{-}L)_4$ are very similar (mF_u = 96.3 and 93.4 pN for the homo and the heteropolyproteins, respectively, Figure 2E). Notably, only 5 OFP experiments were required to reach a lower RSD than in TFP, which is a 3 times higher speed of data acquisition (Figure 2C,E, Supplementary Figure 7A).

Dual-marker orthogonal fingerprinting overcomes confounding protein dimerization

In the AFM experiments reported in Figures 1 and 2, polyproteins are picked up by the cantilever through non-specific physisorption. Hence, experimental traces can contain different number of unfolding events (Figures 1A, 2B). Non-specific protein pickup also leads to the occasional appearance of traces containing more unfolding events than engineered domains comprise the polyprotein, an effect that results from polyprotein dimerization [27]. For instance, in Figure 2B a few traces with n(24 nm) > 8 are identified when pulling from $(C3)_8$. Comparison of Figures 2B and 2D identifies a new population of events at n(24nm) > 4 and n(16nm) > 1 that appear only when $(C3)_8$ and $(C3\text{-}L)_4$ are measured simultaneously, which we interpret as heterodimers between $(C3)_8$ and $(C3\text{-}L)_4$. In the context of OFP, heterodimerization may hamper proper identification of events, since a fraction of C3 unfolding events coming from $(C3)_8$ could be mistakenly assigned to $(C3\text{-}L)_4$ due to the non-zero probability that some dimers are included in the gating region.

In general, the degree of protein dimerization in AFM is dependent on the particular experimental conditions. Hence, heterodimerization poses a challenge to OFP, whose extent may vary depending on the system to study. However, we hypothesized that difficulties coming from protein dimerization could be overcome by using a second protein marker, since traces originating from dimers would be fingerprinted by the presence of both marker proteins. We chose the protein SUMO1 as a second marker because its unfolding length is different from those ones of C3 and protein L [28]. We engineered the heteropolyprotein $(C3\text{-}SUMO1)_4$ and pulled it in the AFM (Supplementary Figure 2). Two population of unfolding steps, at 20 nm and 24 nm are detected, corresponding to the unfolding of SUMO1 and C3, respectively (Supplementary Figure 3C).

Having two marker proteins enables gating criteria that are based exclusively on the presence of the marker domains, in a manner that protein dimers can be identified and excluded from the analysis (Figure 3A,B, Supplementary Figure 8). According to experiments in which $(C3\text{-}L)_4$ and $(C3\text{-}SUMO1)_4$ are measured separately, we used the gating criterion that n(16nm) > 1 and n(20nm) = 0 marks unfolding of $(C3\text{-}L)_4$, and n(20nm) > 1 and n(16nm) = 0 defines unfolding of $(C3\text{-}SUMO1)_4$, which only misclassifies 1 out of 136 traces. Following this gating criterion, which ensures that no dimers are included in the OFP analysis, we determined the distribution of unfolding forces of C3 in the context of $(C3\text{-}SUMO1)_4$ and compared the results with C3 unfolding in the context of $(C3\text{-}L)_4$, both in TFP and OFP (Figure 3C,D). Although the mF_u of C3 in $(C3\text{-}SUMO1)_4$ appears to be lower in TFP experiments (mF_u = 88.4 and 79.2 pN for the L- and SUMO1-containing heteropolyproteins, respectively), differences vanish in OFP experiments (mF_u = 90.0 and 89.5 pN for the L- and SUMO1-containing heteropolyproteins, respectively). The RSD of the distribution of ΔmF_u, as estimated from Monte Carlo simulations fed with the actual number of experiments and events, is 2-3 times smaller in OFP than in TFP,

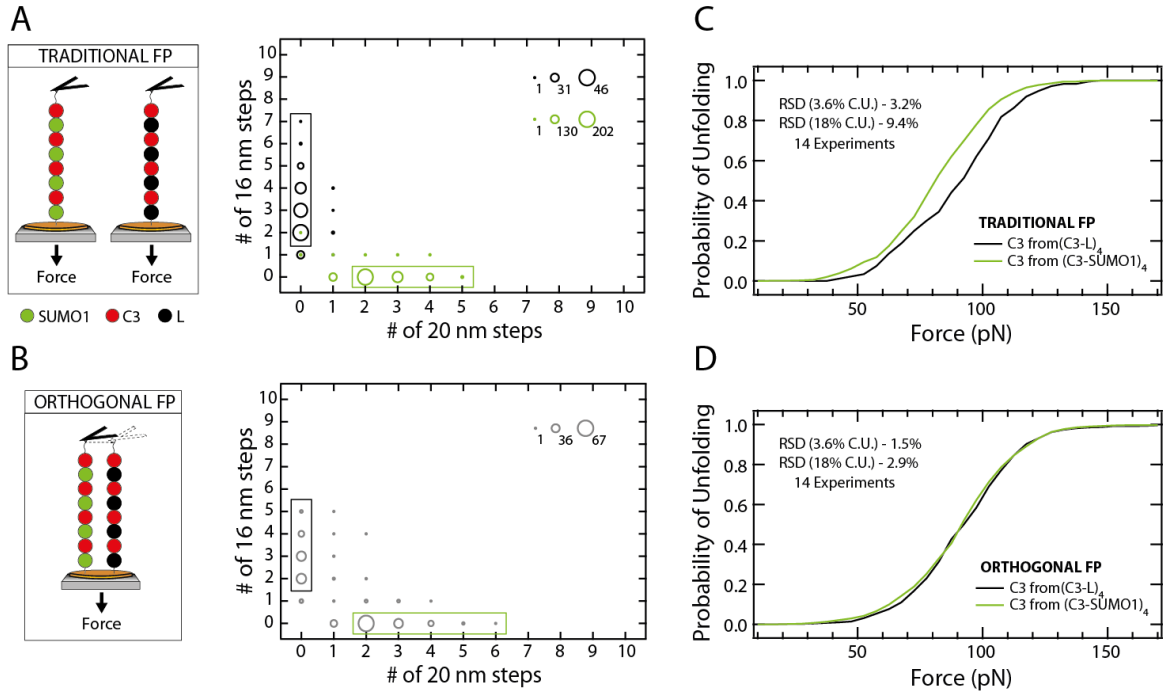

Figure 3. Dual-marker orthogonal fingerprinting overcomes confounding protein dimerization in AFM experiments. (A) Mechanical unfolding of $(C3\text{-}SUMO1)_4$ and $(C3\text{-}L)_4$ are measured in separate experiments by TFP. Individual traces are classified according to their number of 16 and 20 nm unfolding events, which mark the mechanical unfolding of protein L and SUMO1, respectively. The plot shows the frequency of the traces that have different combination of unfolding events, as indicated by the size of the dots. Traces coming from mechanical unfolding of $(C3\text{-}SUMO1)_4$ are assigned when n(16nm) = 0 and n(20nm) > 1 (green rectangle), whereas $(C3\text{-}L)_4$ events are identified by n(16nm) > 1 and n(20nm) = 0. **(B)** Mechanical unfolding of $(C3\text{-}SUMO1)_4$ and $(C3\text{-}L)_4$, as measured in OFP experiments. The gating strategy defined in panel A allows the classification of the traces as originating from $(C3\text{-}SUMO1)_4$ or $(C3\text{-}L)_4$. **(C)** Experimental cumulative unfolding probability distribution of the C3 domain in the context of $(C3\text{-}L)_4$ (6 experiments, 177 events, black) and $(C3\text{-}SUMO1)_4$ (8 experiments, 742 events, green), as measured in TFP. **(D)** Experimental cumulative unfolding probability distribution of the C3 domain in the context of $(C3\text{-}L)_4$ (873 events, black) and $(C3\text{-}SUMO1)_4$ (1043 events, green), calculated from unfolding data obtained in 14 independent orthogonal FP experiments. RSD values in panels C and D are estimated using Monte Carlo simulations that consider extreme values of calibration uncertainty (C.U.) (see also Supplementary Figure 7B). The pulling rate in all experiments was 40 pN/s.

depending on the level of calibration uncertainty (Figure 3C,D and Supplementary Figure 7B, Supplementary Table 1)

Symmetrization of orthogonal fingerprinting datasets improves accuracy

To understand why the improvement in accuracy is preserved when multiple OFP experiments are averaged (Figure 1D), we propose a model for the propagation of calibration errors in AFM experiments conducted under OFP. Considering that every unfolding force measured in the AFM is affected by an error δ, the following equation for the measured ΔmF_u can be derived (Supplementary Text 3):

$$\Delta mF_u^{measured} = \Delta mF_u^{real} + \sum_{j=1}^{n_{exp}} \bar{\delta}_j \cdot \left(\frac{n_{prot1,j}}{n_{events,prot1}} - \frac{n_{prot2,j}}{n_{events,prot2}} \right) \qquad \textit{Equation 1}$$

In Equation 1, ΔmF_u^{real} is the value of ΔmF_u that would be measured if there was no error in calibration, n_{exp} is the number of OFP experiments, $n_{prot1,j}$ and $n_{prot2,j}$ are the number of unfolding events for both proteins being compared in experiment j, $n_{events,prot1}$ and

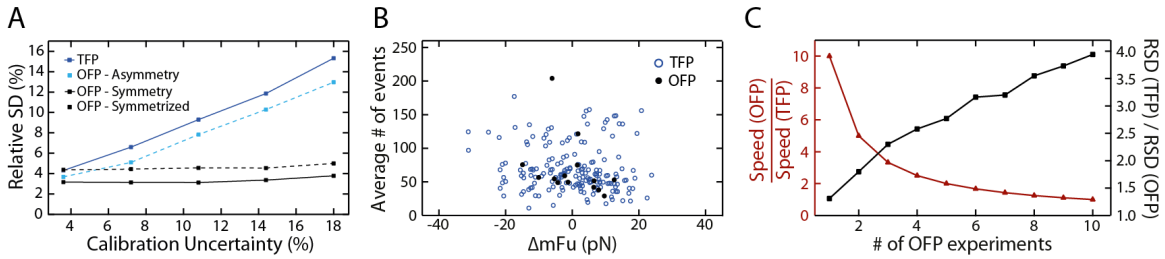

Figure 4. Improved accuracy and throughput of orthogonal fingerprinting. (A) Monte Carlo simulations show that symmetrization of datasets obtained under OFP improves RSD of distributions of ΔmF_u at high calibration uncertainties. Symmetric simulations (solid lines, 100 events per experiment and protein) considered 2 experiments per protein in TFP (blue), and 2 experiments in OFP (black). To simulate asymmetric OFP datasets, uneven number of unfolding events (50/150) were considered for both proteins in the first simulated experiment, and the order was reversed in the second simulated experiment (dashed blue line, see text). Symmetrization was examined by running simulations at the lowest number of events for both experiments (50, dashed black line). **(B)** The experimental mF_u of C3 in the context of $(C3\text{-}L)_4$ and $(C3\text{-}SUMO1)_4$ is compared in 14 individual OFP experiments, and the corresponding ΔmF_u is represented (solid black circles). Using the same dataset, the equivalent ΔmF_u in traditional AFM was calculated from pairwise comparison of mF_u values from different experiments (open blue circles). **(C)** Improvement in the speed of data acquisition (red) and RSD in the distribution of ΔmF_u (black) are estimated using Monte Carlo simulations at 10.8% calibration uncertainty (100 events per experiment and protein). The reference is a situation where the mechanical properties of two proteins are measured in 5 traditional experiments per protein.

$n_{events,prot2}$ are the total number of unfolding events for each protein, and $\bar{\delta}_j$ is the average value of the error in force in experiment j, which, as a consequence of OFP, is considered to be equivalent for both proteins.

Equation 1 shows that in OFP, $\Delta mF_u(measured)$ is distributed around $\Delta mF_u(real)$ according to the magnitude of $\bar{\delta}_j$ values, which are set by the uncertainty of cantilever calibration, and by how the unfolding events are distributed among the different experiments. Importantly, if the proportion of events for both proteins is constant in every experiment of the dataset ("symmetry" condition: $n_{prot1,j} = constant \cdot n_{prot2,j}$), Equation 1 leads to $\Delta mF_u(measured) = \Delta mF_u(real)$, i.e. the measured force is not affected by errors in calibration. Our Monte Carlo simulations readily confirm this prediction. While simulations of 2 OFP experiments with 100 events per protein show that the resulting RSD in ΔmF_u does not depend on the uncertainty in calibration, breaking the symmetry by considering $n_{prot1,1} = n_{prot2,2} = 150$ and $n_{prot1,2} = n_{prot2,1} = 50$, results in a dramatic increase of RSD especially at higher calibration uncertainties (Figure 4A). Indeed, under these asymmetry conditions, the performance of OFP drastically diminishes and the obtained RSD approaches the one obtained by TFP (Figure 4A).

Since asymmetric data result in poorer performance of OFP, we examined whether symmetrization of OFP datasets results in improved RSD. To simulate symmetrization, we did Monte Carlo simulations of 2 OFP experiments in which $n_{prot1,j} = n_{prot2,j} = 50$, i.e. we trimmed 100 extra events per protein so that both experiments had the same number of events for both proteins. Even though having less events per experiment results *per* se in poorer definition of distributions of unfolding forces (Figure 1C, Supplementary Figure 5B), the resulting RSD of ΔmF_u after symmetrization becomes independent of the calibration uncertainty and is lower than the RSD of the more populated, asymmetric dataset at calibration uncertainties higher than 7% (Figure 4A).

We have tested the effect of symmetrization in our real AFM datasets by removing unfolding events so that every OFP experiment verifies the symmetry condition $n_{prot1} = n_{prot2}$. Feeding Monte Carlo simulations with these trimmed datasets, we estimate that the RSD of the distribution of ΔmF_u of the symmetrized datasets becomes lower than the original RSD also at calibration uncertainties higher than 7% (Supplementary Figure 7), although in both examples the differences between the asymmetry and the symmetrized conditions is less prominent than in Figure 4A. Indeed, we find that the extent of improvement in RSD by symmetrization depends on the number of experiments performed (Supplementary Figure 9) together with the degree of asymmetry as predicted by Equation 1. Hence, we recommend that improvement in RSD by symmetrization is evaluated on a case-by-case basis using Monte Carlo simulations as we have done here.

DISCUSSION

Comparisons of unfolding forces are required to examine the effect of mutations, posttranslational modifications and chemical environment in the mechanical stability of proteins and their complexes, and to assign mechanical hierarchies in multidomain, elastic proteins [17-19,23,29,30]. Traditionally, these mechanical comparisons have been hampered by errors associated with force calibration in AFM. Here, we have developed widely-adaptable orthogonal fingerprinting strategies to compare the mechanics of proteins by single-molecule AFM. Our new method outperforms traditional AFM in three key aspects (Figures 4, 5):

(i) The accuracy of OFP is independent of calibration uncertainty even when multiple experiments are averaged (Figures 1F,4A, Supplementary Figure 6). Although the uncertainty of cantilever calibration by the thermal fluctuations method is usually considered to lie in the range of 15-20% [14], the real uncertainty is extremely challenging to estimate. We have provided a lower bound of 3.6% uncertainty by measuring the variation of calibration parameters for a single cantilever (Supplementary Text 2). Uncertainties in spring constant calibration have also been estimated by interlaboratory experiments, finding a value of up to 11% [31]. However, neither of these approaches addresses more fundamental assumptions of the calibration procedures that can lead to higher calibration uncertainties [32]. The impact of OFP with respect to traditional AFM that is summarized in Figure 5 considers a realistic calibration uncertainty of 10.8%. However, it is important to note that due to its insensitiveness to calibration errors, OFP avoids the effects of force miscalibrations that originate from difficult-to-detect defects in specific cantilevers. Furthermore, the impact of OFP may be more relevant in the light of the availability of next generation cantilevers, which are pushing the AFM limits into ranges of forces, stability and time resolutions that are not accessible to conventional cantilevers [33-36]. These high-performance cantilevers are more challenging to calibrate [13], so we envision that combination of OFP strategies and these new cantilevers is set to expand the reach of single-molecule AFM.

(ii) OFP shows much improved accuracy (Figures 1E,F, 4A,C). This increase in accuracy captured by Monte Carlo simulations is also observed in our experimental dataset, since the spread of ΔmF_u in pairs of OFP experiments is lower than in TFP experiments (SD = 8.0 *vs* 11.2 pN, respectively) (Figure 4B). Keeping the speed of data acquisition constant at high calibration uncertainties, the RSD achieved by OFP can be 6 times lower than in TFP (Figure 5, Supplementary Figure 6B).

(iii) The throughput of OFP is much increased. We estimate that OFP can obtain the same accuracy more than 30 times faster than TFP at high calibration uncertainties (Supplementary Figure 6C). In addition, proteins to be probed in OFP can be purified simultaneously

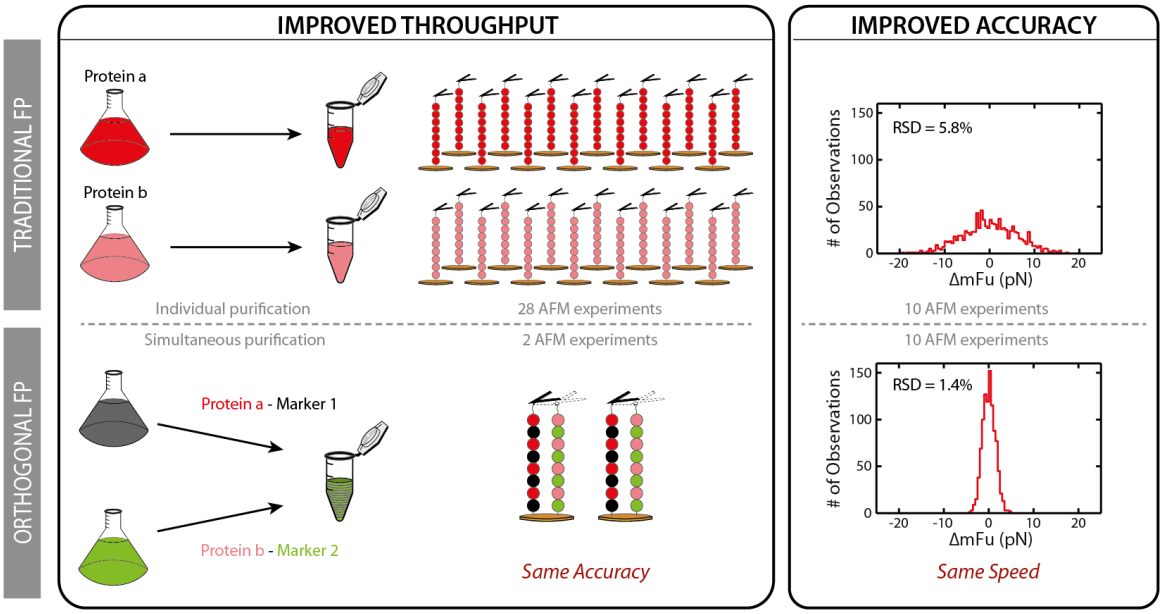

Figure 5. Overview of orthogonal fingerprinting force-spectroscopy AFM. In the traditional approach, comparison of the mechanical stability of *Protein a* and *Protein b* involves independent purification and several AFM experiments to compensate for inaccurate force calibration. OFP is based on the production of heteropolyproteins composed of the proteins of interest fused to marker domains. Since the markers provide unequivocal fingerprints in single-molecule pulling experiments, OFP enables simultaneous purification and measurement in the AFM, circumventing errors in force calibration. Hence, OFP can achieve the same accuracy as conventional single-molecule AFM with much better throughput (*left*). Alternatively, by keeping the speed of data acquisition constant, OFP considerably improves the accuracy of single-molecule AFM (*right*). The improvement in throughput and accuracy are estimated from simulations at 10.8% calibration uncertainty (100 events per experiment and protein).

(Supplementary Figures 2, 10), which results in extra savings in working time and reagents while ensuring equal experimental conditions for both proteins (Figure 5).

The increase in throughput and accuracy of OFP come at the expense of each other. Hence, depending on the goals of an OFP study, the experimenter can choose to favor one or the other, or to find a balance between both. In this regard, our Monte Carlo simulations can help experimental design (code is provided as Supplementary Material). For instance, in Figure 4C, we show that different gains in accuracy and throughput can be achieved depending on the number of OFP experiments chosen to compare two proteins, considering 10 TFP experiments as a reference.

A direct application of OFP is to examine how neighboring domains affect protein nanomechanics. Indeed, the use of heteropolyproteins relies on the assumption that the effect of neighboring domains in the mechanics of a protein domain is negligible [26,37-39]. Our highly accurate OFP experiments show that the mechanical stabilities of the C3 domain in the context of a $(C3)_8$ homopolyprotein, or within a $(C3\text{-}L)_4$ or $(C3\text{-}SUMO1)_4$ heteropolyproteins, are very similar (Figures 2, 3). Hence, our data lend strong support to the use of heteropolyproteins in force-spectroscopy AFM. In particular, since the mechanical properties of the C3 domain are independent of the flanking domains, the mechanical effects of mutations in C3 that cause heart disease can be directly tested using OFP strategies [40].

Simultaneous mechanical characterization of proteins has been achieved before combining microfluidics, on-chip protein expression and AFM measurements in a combined atomic

force/total internal reflection fluorescence microscope [15,22]. An advantage of OFP is that it can be readily implemented in any force-spectroscopy AFM setup. In addition, different fingerprinting lengths provide additional reassurance of the identity of the probed molecules. In this regard, OFP is very well suited to compare mechanical properties of proteins with similar unfolding lengths, such as mutants of the same protein[17,19]. In those cases where the proteins to compare have different unfolding lengths, simultaneous measurement is of immediate application and can lead to the increase in accuracy and throughput described here. Examples include examination of the effect of disulfide bonds, protein misfolding, multimerization, and pulling geometry in the mechanical stability of proteins and their complexes [41-48], and determination of rates of force-activated chemical reactions [49]. In these examples, our Monte Carlo simulations and theoretical developments can be fully applied to guide experimental design and interpretation.

Orthogonal fingerprinting can be further improved in two aspects. Since the relative performance of OFP is better at high number of events (Figure 1E, Supplementary Text 4), we propose that even better accuracy will be achieved by combining OFP with high-strength single-molecule tethering strategies, which can capture more unfolding events per experiment [22,27,50]. In addition, OFP strategies hold the promise of further parallelization by the use of multiple marker proteins, which can take high resolution force-spectroscopy AFM to the realm of high-throughput single-molecule techniques [51].

METHODS

Monte Carlo simulations

Monte Carlo simulations were programmed in Igor 6 (Wavemetrics). Code is available as Supplementary Material. Simulations randomly assign an error in force according to a set uncertainty in the calibration between 3.6% and 18% (Supplementary Text 2). Every simulated AFM experiment is therefore affected by a different calibration error, except under the condition of OFP, in which two proteins are measured in the same AFM experiment and share error in force. Each cycle of the simulations obtains a value of ΔmF_u of two proteins from Gaussian fits to their distribution of unfolding forces, which are obtained from a given number of independent experiments and unfolding events. We used a bin size of 25 pN when simulating artificial datasets, or 5 pN when feeding simulations with real datasets for better comparison with experimental distributions of unfolding forces. Simulations return the RSD of the ΔmF_u distribution obtained from 1,000 cycles of the Monte Carlo procedure. To calculate RSD, we consider the SD of the distribution, and normalize it according to the theoretical value of mF_u [52].

Distributions of unfolding forces are calculated through a kinetic Monte Carlo routine that considers that protein unfolding is exponentially dependent on force according to the Bell's model [53]:

$$r = r_0 \cdot e^{F \cdot \Delta x / k_b \cdot T} \qquad \textit{Equation 2}$$

In Equation 2, r is the rate of protein unfolding, r_0 is the rate of unfolding at zero force, F is the force experienced by the protein, Δx is the distance to the transition state, k_b is the Boltzmann constant and T is the absolute temperature. In the simulations, we considered that $k_b \cdot T$ = 4.11 pN·nm, r_0 = 0.2 nm and Δx = 0.01 s^{-1}. We chose these values because they are a good estimate of mechanical unfolding parameters of C3. We checked that values of RSD are fairly insensitive to small variations in r_0 and Δx and therefore one single set of parameters is enough to calculate

RSD of distributions of ΔmF_u even if the mechanical parameters of the proteins to be compared are slightly different (Supplementary Table 2).

The kinetic Monte Carlo routine to obtain distribution of unfolding forces compares a random number with the instant probability of unfolding at a given force. If the unfolding probability is higher than the random number, unfolding is considered to happen at that force. Instant probabilities of unfolding are calculated following a linear approximation according to reference [54]:

$$P_u = n \cdot r_0 \cdot e^{F \cdot \varepsilon \cdot \Delta x / k_b \cdot T} \cdot \Delta t \qquad \textit{Equation 3}$$

In Equation 3, n is the number of domains that remain folded at a particular force, ε is the error in force due to the uncertain cantilever calibration (Supplementary Text 2) and Δt is the time step of the Monte Carlo. In the simulations, we used $\Delta t = 10^{-4}$ s, which ensures validity of the linear approximation, since $n \cdot r \cdot \Delta t$ is kept under 0.05 (Supplementary Text 5). Pilot simulations show that results do not vary if we use a smaller time step of $\Delta t = 10^{-5}$ s.

Protein production and purification

The cDNAs coding for the C3-L and C3-SUMO1 constructs were produced by gene synthesis (NZY-Tech and Gene Art, respectively). The cDNA coding for the C3 domain was obtained by PCR. cDNAs coding for polyproteins were produced following an iterative strategy of cloning using BamHI, BglII and KpnI, as described before [25,55]. Final cDNAs were inserted in the pQE80L expression plasmid using BamHI and KpnI and the resulting plasmids were verified by Sanger sequencing. Full protein sequences are reported in Supplementary Text 1. Polyproteins were expressed in BLR (DE3) *E. coli* strain. Briefly, fresh cultures (OD_{600} = 0.6-1.0) are induced with 1mM IPTG for 3 hours at 37ºC and at 250 rpm. Cells are lysed by a combination of tip sonication and passes through a French Press. Polyproteins are purified from the soluble fraction through Ni-NTA agarose chromatography (Qiagen), following the recommendations of the supplier and adding 10 mM DTT to the buffers. Further purification is achieved by size-exclusion chromatography in an AKTA Pure 25L system using a Superose 6 Increase 10/300 GL or a Superdex 200 Increase 10/300 GL column (GE Healthcare). The proteins are eluted in 10 mM Hepes, pH 7.2, 150 mM NaCl, 1 mM EDTA, which is also the buffer used in AFM experiments. Purity of samples was evaluated using SDS-PAGE gels (a typical result is shown in Supplementary Figure 2).

Force-spectroscopy by AFM

Single-molecule AFM measurements were obtained in a force-clamp AFS (Luigs & Neumann) according to established protocols [11].We used silicon nitride MLCT-C cantilevers with a 60-nm gold back side coating (Bruker), which were calibrated according to the thermal fluctuations method [56]. Typical spring constant values ranged between 15 and 20 pN/nm. A small aliquot (2-10 µL) of the purified protein is deposited on the surface of a gold coated cover slip (Luigs & Neumann), or directly into the Hepes buffer contained in the fluid chamber of the AFS. The cantilever is brought in contact to the surface for 1-2 s at 500-2000 pN to favor formation of single-molecule tethers. Then, the surface is retracted to achieve the set point force. If a single-molecule tether is formed, the force is increased linearly at 40 pN/s for 5 s while the length of the polyprotein is measured. This protocol ensures full unfolding of C3, L and SUMO1 domains (Supplementary Figure 3). Unfolding events are detected as increases in the length of the protein. In the initial characterization of polyproteins, we analyze all traces that contain at least

two events of the same size, which allows to set a fingerprinting length for the domains (24 ± 1 nm for C3, 16 ± 1 nm for protein L, and 20 ± 1 nm for SUMO1, see Supplementary Figure 3). For the rest of the analyses, we only considered traces that contain fingerprinting unfolding lengths. Unfolding forces were recorded and plotted as cumulative distributions. mF_u values were obtained from Gaussian fits to histograms of unfolding forces. Force inaccuracy due to laser interference was lower than 40 pN in all experiments (peak-to-peak height in baseline force-extension recordings) [11].

Author contributions

J.A.C. designed the research. D.V.C engineered polyprotein constructs and produced proteins. C.P.L., C.S.C and D.S.O. did AFM experiments and analyzed single-molecule data. J.A.C programmed Monte Carlo simulations. C.P.L., C.S.C and J.A.C. run and analyzed Monte Carlo simulations and assembled display figures. J.A.C. wrote the manuscript with input from all the authors.

Acknowledgements

J.A.C. acknowledges funding from the Spanish Ministry of Economy, Industry and Competitiveness (MINECO) through grants BIO2014-54768-P, BIO2017-83640-P, and RYC-2014-16604, the European Research Area Network on Cardiovascular Diseases (ERA-CVD, MINOTAUR, AC16/00045), and the CNIC intramural grant program (03-2016 IGP). The CNIC is supported by MINECO and the Pro CNIC Foundation, and is a Severo Ochoa Center of Excellence (MINECO award SEV-2015-0505). C.P.L. was a recipient of CNIC Master Fellowship. C.S.C. is the recipient of an FPI predoctoral fellowship BES-2016-076638. We thank Natalia Vicente for excellent technical support. We thank all the members of the laboratory of Molecular Mechanics of the Cardiovascular System for helpful discussions. We thank Elías Herrero-Galán (CNIC, Madrid) for critical reading of the manuscript and Lidia Prieto-Frías for key insights about propagation of calibration errors.

Competing financial interests

The authors declare no competing financial interest.

Resources

The code used for the Monte Carlo simulations is available as online Supplementary Material.

REFERENCES

1.Linke, W. A. *et al.* Gigantic business: titin properties and function through thick and thin. *Circ Res* **114**, 1052-1068. (2014).

2.del Rio, A. *et al.* Stretching single talin rod molecules activates vinculin binding. *Science* **323**, 638-641. (2009).

3.Paluch, E. K. *et al.* Mechanotransduction: use the force(s). *BMC biology* **13**, 47. (2015).

4.Li, H. *et al.* Reverse engineering of the giant muscle protein titin. *Nature* **418**, 998-1002. (2002).

5.Thomas, W. E. *et al.* Bacterial adhesion to target cells enhanced by shear force. *Cell* **109**, 913-923. (2002).

6.Thomas, W. E. *et al.* Biophysics of catch bonds. *Annual review of biophysics* **37**, 399-416. (2008).

7.Strohmeyer, N. *et al.* Fibronectin-bound α5β1 integrins sense load and signal to reinforce adhesion in less than a second. *Nat Mater* **16**, 1262. (2017).

8.Lv, S. *et al.* Designed biomaterials to mimic the mechanical properties of muscles. *Nature* **465**, 69-73. (2010).

9.Harden, J. L. *et al.* Editorial: Special Issue on Designer Protein Biomaterials. *ACS Biomaterials Science & Engineering* **3**, 658-660. (2017).

10.Neuman, K. C. *et al.* Single-molecule force spectroscopy: optical tweezers, magnetic tweezers and atomic force microscopy. *Nat Methods* **5**, 491-505. (2008).

11.Popa, I. *et al.* Force dependency of biochemical reactions measured by single-molecule force-clamp spectroscopy. *Nat Protoc* **8**, 1261-1276. (2013).

12.Rief, M. *et al.* Reversible unfolding of individual titin immunoglobulin domains by AFM. *Science* **276**, 1109-1112. (1997).

13.Slattery, A. D. *et al.* Spring constant calibration techniques for next-generation fast-scanning atomic force microscope cantilevers. *Nanotechnology* **25**, 335705. (2014).

14.Charles, A. C. *et al.* The determination of atomic force microscope cantilever spring constants via dimensional methods for nanomechanical analysis. *Nanotechnology* **16**, 1666. (2005).

15.Otten, M. *et al.* From genes to protein mechanics on a chip. *Nat Methods* **11**, 1127-1130. (2014).

16.Alegre-Cebollada, J. *et al.* S-glutathionylation of cryptic cysteines enhances titin elasticity by blocking protein folding. *Cell* **156**, 1235-1246. (2014).

17.Li, H. *et al.* Point mutations alter the mechanical stability of immunoglobulin modules. *Nat Struct Biol* **7**, 1117-1120. (2000).

18.Li, H. *et al.* Atomic force microscopy reveals the mechanical design of a modular protein. *Proc Natl Acad Sci U S A* **97**, 6527-6531. (2000).

19.Williams, P. M. *et al.* Hidden complexity in the mechanical properties of titin. *Nature* **422**, 446-449. (2003).

20.Anderson, B. R. *et al.* Single molecule force spectroscopy on titin implicates immunoglobulin domain stability as a cardiac disease mechanism. *J Biol Chem* **288**, 5303-5315. (2013).

21.Sadler, D. P. *et al.* Identification of a mechanical rheostat in the hydrophobic core of protein L. *J Mol Biol* **393**, 237-248. (2009).

22.Verdorfer, T. *et al.* Combining in Vitro and in Silico Single-Molecule Force Spectroscopy to Characterize and Tune Cellulosomal Scaffoldin Mechanics. *Journal of the American Chemical Society* **139**, 17841-17852. (2017).

23.Jobst, M. A. *et al.* Resolving dual binding conformations of cellulosome cohesin-dockerin complexes using single-molecule force spectroscopy. *eLife* **4**(2015).

24.Carrion-Vazquez, M. *et al.* Mechanical design of proteins studied by single-molecule force spectroscopy and protein engineering. *Prog Biophys Mol Biol* **74**, 63-91. (2000).

25.Carrion-Vazquez, M. *et al.* Mechanical and chemical unfolding of a single protein: a comparison. *Proc Natl Acad Sci U S A* **96**, 3694-3699. (1999).
26.Li, H. *et al.* Multiple conformations of PEVK proteins detected by single-molecule techniques. *Proc Natl Acad Sci U S A* **98**, 10682-10686. (2001).
27.Popa, I. *et al.* Nanomechanics of HaloTag tethers. *Journal of the American Chemical Society* **135**, 12762-12771. (2013).
28.Kotamarthi, H. C. *et al.* Single-molecule studies on PolySUMO proteins reveal their mechanical flexibility. *Biophys J* **104**, 2273-2281. (2013).
29.Oroz, J. *et al.* The Y9P Variant of the Titin I27 Module: Structural Determinants of Its Revisited Nanomechanics. *Structure* **24**, 606-616. (2016).
30.Oberhauser, A. F. *et al.* The mechanical hierarchies of fibronectin observed with single-molecule AFM. *J Mol Biol* **319**, 433-447. (2002).
31.te Riet, J. *et al.* Interlaboratory round robin on cantilever calibration for AFM force spectroscopy. *Ultramicroscopy* **111**, 1659-1669. (2011).
32.Ohler, B. Practical Advice on the Determination of Cantilever Spring Constants. Veeco Instruments Incorporated, Technical Report., (2007).
33.Rico, F. *et al.* High-speed force spectroscopy unfolds titin at the velocity of molecular dynamics simulations. *Science* **342**, 741-743. (2013).
34.Yu, H. *et al.* Hidden dynamics in the unfolding of individual bacteriorhodopsin proteins. *Science* **355**, 945-950. (2017).
35.He, C. *et al.* Direct Observation of the Reversible Two-State Unfolding and Refolding of an alpha/beta Protein by Single-Molecule Atomic Force Microscopy. *Angew Chem Int Ed Engl* **54**, 9921-9925. (2015).
36.Faulk, J. K. *et al.* Improved Force Spectroscopy Using Focused-Ion-Beam-Modified Cantilevers. *Methods Enzymol* **582**, 321-351. (2017).
37.Dietz, H. *et al.* Exploring the energy landscape of GFP by single-molecule mechanical experiments. *Proc Natl Acad Sci U S A* **101**, 16192-16197. (2004).
38.Steward, A. *et al.* Versatile cloning system for construction of multimeric proteins for use in atomic force microscopy. *Protein Science* **11**, 2179-2183. (2002).
39.Oroz, J. *et al.* Unequivocal Single-Molecule Force Spectroscopy of Proteins by AFM Using pFS Vectors. *Biophys J* **102**, 682-690. (2012).
40.Harris, S. P. *et al.* In the thick of it: HCM-causing mutations in myosin binding proteins of the thick filament. *Circ Res* **108**, 751-764. (2011).
41.Giganti, D. *et al.* Disulfide isomerization reactions in titin immunoglobulin domains enable a mode of protein elasticity. *Nat Commun* **9**, 185. (2018).
42.Manteca, A. *et al.* Mechanochemical evolution of the giant muscle protein titin as inferred from resurrected proteins. *Nat Struct Mol Biol* **24**, 652-657. (2017).
43.Manteca, A. *et al.* The influence of disulfide bonds on the mechanical stability of proteins is context dependent. *J Biol Chem* **292**, 13374-13380. (2017).
44.Bertz, M. *et al.* Mechanical stability of the antibody domain CH3 homodimer in different oxidation states. *J Am Chem Soc* **135**, 15085-15091. (2013).
45.Carrion-Vazquez, M. *et al.* The mechanical stability of ubiquitin is linkage dependent. *Nat Struct Biol* **10**, 738-743. (2003).
46.Oberhauser, A. F. *et al.* Single protein misfolding events captured by atomic force microscopy. *Nat Struct Biol* **6**, 1025-1028. (1999).
47.Sarkar, A. *et al.* The mechanical fingerprint of a parallel polyprotein dimer. *Biophys J* **92**, L36-38. (2007).
48.Carl, P. *et al.* Forced unfolding modulated by disulfide bonds in the Ig domains of a cell adhesion molecule. *Proc Natl Acad Sci U S A* **98**, 1565-1570. (2001).
49.Garcia-Manyes, S. *et al.* Force-activated reactivity switch in a bimolecular chemical reaction. *Nat Chem* **1**, 236-242. (2009).

50.Zakeri, B. *et al.* Peptide tag forming a rapid covalent bond to a protein, through engineering a bacterial adhesin. *Proc Natl Acad Sci U S A* **109**, E690-697. (2012).
51.Hill, F. R. *et al.* The more the merrier: high-throughput single-molecule techniques. *Biochemical Society transactions* **45**, 759-769. (2017).
52.Schlierf, M. *et al.* The unfolding kinetics of ubiquitin captured with single-molecule force-clamp techniques. *Proc Natl Acad Sci U S A* **101**, 7299-7304. (2004).
53.Bell, G. I. Models for the specific adhesion of cells to cells. *Science* **200**, 618-627. (1978).
54.Shi, J. *et al.* Simulated data sets for single molecule kinetics: some limitations and complications of data analysis. *European biophysics journal : EBJ* **35**, 633-645. (2006).
55.Alegre-Cebollada, J. *et al.* Isopeptide bonds block the mechanical extension of pili in pathogenic Streptococcus pyogenes. *J Biol Chem* **285**, 11235-11242. (2010).
56.Hutter, J. L. *et al.* Calibration of atomic-force microscope tips. *Review of Scientific Instruments* **64**, 1868-1873. (1993).